22. Rypma, B. & D'Esposito, M. D. A subsequent-memory effect in dorsolateral prefrontal cortex. *Cogn. Brain Res.* **16,** 162–166 (2003).
23. Rypma, B., Prabhakaran, V., Desmond, J., Glover, G. H. & Gabrieli, J. D. Load-dependent roles of frontal brain regions in the maintenance of working memory. *Neuroimage* **9,** 216–226 (1999).
24. Eriksen, C. W. & St James, J. D. Visual attention within and around the field of focal attention: A zoom lens model. *Percept. Psychophys.* **40,** 225–240 (1986).
25. Pashler, H. Familiarity and visual change detection. *Percept. Psychophys.* **44,** 369–378 (1988).
26. Logie, R. H. *Visuo-Spatial Working Memory* (Erlbaum, Hove, UK, 1995).
27. Kane, M. J. & Engle, R. W. Working memory capacity and the control of attention: The contributions of goal neglect, response competition, and task set to Stroop interference. *J. Exp. Psychol. Gen.* **132,** 47–70 (2003).
28. Daneman, M. & Merikle, P. M. Working memory and language comprehension: A meta-analysis. *Psychon. Bull. Rev.* **3,** 422–433 (1996).
29. Kyllonen, P. C. & Christal, R. E. Reasoning ability is (little more than) working memory capacity. *Intelligence* **14,** 398–433 (1990).
30. Vogel, E. K., Luck, S. J. & Shapiro, K. L. Electrophysiological evidence for a postperceptual locus of suppression during the attentional blink. *J. Exp. Psychol. Hum. Percept. Perform.* **24,** 1656–1674 (1998).

Acknowledgements The research reported here was supported by a grant from the US National Institute of Mental Health.

Competing interests statement The authors declare that they have no competing financial interests.

Correspondence and requests for materials should be addressed to E.K.V. (vogel@darkwing.uoregon.edu).

Capacity limit of visual short-term memory in human posterior parietal cortex

J. Jay Todd & René Marois

Vanderbilt Vision Research Center, Department of Psychology, Vanderbilt University, 530 Wilson Hall, Nashville, Tennessee 37203, USA

At any instant, our visual system allows us to perceive a rich and detailed visual world. Yet our internal, explicit representation of this visual world is extremely sparse: we can only hold in mind a minute fraction of the visual scene[1,2]. These mental representations are stored in visual short-term memory (VSTM). Even though VSTM is essential for the execution of a wide array of perceptual and cognitive functions[3–5], and is supported by an extensive network of brain regions[6–9], its storage capacity is severely limited[10–13]. With the use of functional magnetic resonance imaging, we show here that this capacity limit is neurally reflected in one node of this network: activity in the posterior parietal cortex is tightly correlated with the limited amount of scene information that can be stored in VSTM. These results suggest that the posterior parietal cortex is a key neural locus of our impoverished mental representation of the visual world.

To investigate the neural basis of VSTM's storage capacity limit, 17 subjects were scanned while performing a parametric load manipulation[14] of a delayed visual matching-to-sample task (Fig. 1). On each trial, subjects were briefly presented with a sample display containing one to eight coloured discs and, after a 1,200-ms retention interval, decided whether a single probe disc matched one of the sample discs in location and colour. A 1,200-ms delay maximizes VSTM's capacity: with delays shorter than 1 s, VSTM capacity is inflated by sensory (iconic) representations of the display[15], whereas long delays not only underestimate VSTM capacity owing to memory degradation[15], but also favour the recruitment of rehearsal mechanisms and verbal/abstract recoding of the visual material[16]. To minimize verbal strategies further, a verbal working-memory/articulatory suppression task was administered concurrently with the VSTM task: throughout the trial, subjects rehearsed two digits presented at trial onset and reported them at trial offset. Performance in this task was high and independent of VSTM set size (92–94% accuracy across set sizes; $F_{5,80} = 0.64$, $P = 0.67$), attesting to the absence of a trade-off between the verbal and visual tasks, as predicted from the independence of these two working-memory systems[17,18].

Accuracy in the VSTM task declined with increased set size (set size 1, 97.7%; set size 2, 94.2%; set size 3, 90.0%; set size 4, 86.2%; set size 6, 73.3%; set size 8, 68.5%). The number of objects encoded at each set size, estimated with Cowan's K formula[11], increased up to set size 3 or 4, and levelled off thereafter (Fig. 2; t-test between set sizes 4 and 8, $P > 0.05$). This behavioural function is fitted significantly better by a quadratic function than by a linear function ($P = 0.01$)[19]. Thus, VSTM storage capacity is about three or four items, which is consistent with previous studies[11,13]. Importantly, this capacity limit is not due to insufficient time to encode items in VSTM[4]. Tripling the sample presentation time from 150 to 450 ms in a separate experiment did not affect the K function ($n = 16$, $P = 0.28$), an observation consistent with previous findings[12,13]. The VSTM task therefore expresses the capacity limit of VSTM storage as opposed to a limitation in spatially attending to the display or encoding items in VSTM.

The brain substrates mediating VSTM's storage capacity limit should demonstrate a response profile paralleling the behavioural K function: activation should increase until set size 3 or 4 and level off thereafter. To isolate such regions, a voxel-based multiple regression analysis with K-weighted set size coefficients was performed. The resulting statistical parametric maps revealed a single bilaterally symmetric area in the intraparietal and intraoccipital sulci (IPS/IOS; $P < 0.05$ corrected). Time-course analysis (Fig. 3a) confirmed a strong correlation between the IPS/IOS peak response amplitude and the number of objects encoded ($r = 0.54$, $P < 0.001$; Fig. 2). The peak blood oxygenation level-dependent (BOLD) response function reached a plateau by set size 4 (t-test between 4 and 8, $P < 0.05$) and was better described by a quadratic function than by a linear function ($P < 0.01$). This parietal activation is not simply related to task difficulty: accuracy decreased and reaction

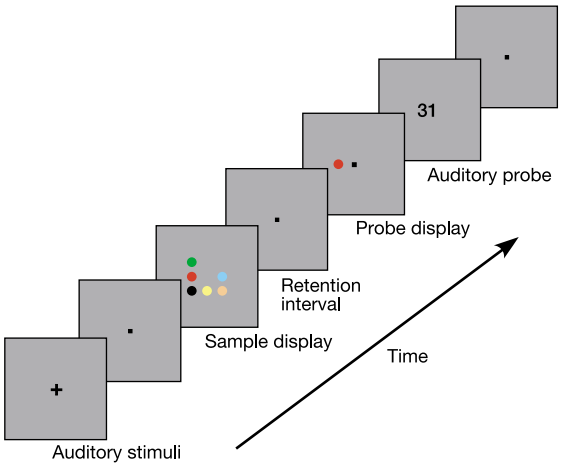

Figure 1 Trial design. Each trial began with the auditory presentation of two digits to be rehearsed throughout the trial. A sample display containing a variable number of coloured discs was then presented for 150 ms, followed by a 1,200-ms retention period, and then by a single coloured probe disc. Subjects judged whether the colour of the probe matched the colour of the disc shown at the same position in the sample display. Afterwards, two digits appeared and subjects indicated whether these were the same as those presented at trial onset.

time increased between set sizes 4 and 8 (P values < 0.05), when IPS/IOS activity and number of objects encoded remained constant. The levelling off of the BOLD signal at 0.3% is also unlikely to have resulted from haemodynamic saturation of the neurovascular system. In four subjects, we observed BOLD responses of more than 0.4% relative to fixation baseline in the same region of interest (ROI) when a working-memory task was presented at a short inter-trial interval (3 s), a condition that increases signal amplitude because of the summation of overlapping individual BOLD responses. Finally, the IPS/IOS involvement in VSTM generalizes across stimulus classes: it was also observed with white bars of varied orientations (0°, 45°, 90°, 135° and 180°) as stimuli (correlation of percentage signal change with K function of 0.64, $P < 0.01$, $n = 4$).

Could IPS/IOS activity reflect the perceptual or iconic representation of the number of objects in the scene instead of the number of objects stored in VSTM? To address this issue, we performed an iconic memory (IM) experiment that was identical to the first one except that for each trial only the sample display was presented, and subjects made an immediate judgement about the presence or absence of a coloured disc in the central position of the display. This task required attending to the display—with all stimuli presented at the fovea—and executing a response, but placed minimal and equal VSTM demands across set sizes. Performance was near ceiling across set sizes (96–98%). Relative to the VSTM experiment, the IPS/IOS BOLD response was attenuated and the set size effect was eliminated ($F_{1,5} = 1.13$, $P = 0.37$; Figs 2 and 3a). Thus, the IPS/IOS is insensitive to the perceptual load of the visual scene.

Visual working-memory tasks are traditionally decomposed into encoding, maintenance and retrieval phases[14,20,21]. If the IPS/IOS is involved in VSTM storage, it should be engaged during maintenance, and not just at encoding or retrieval. Because of the short retention interval used in the VSTM experiment, the IPS/IOS response in each of these phases could not be distinguished. We therefore performed an additional VSTM load experiment with a sufficiently long retention interval (9,200 ms) to dissociate activity related to encoding, maintenance and retrieval[21,22]. Only two set sizes were used to compensate for the lower number of trials acquired in this slow-event paradigm. As expected, the number of objects encoded at set size 3 was higher than at set size 1 ($K = 2.12$ versus 0.91, $P < 0.05$). Correspondingly, the IPS/IOS ROI was more activated at the larger set size during both encoding and maintenance (P values < 0.05, one-tailed) but not during retrieval ($P > 0.05$; Fig. 4). Thus, the IPS/IOS is sensitive to working-memory load chiefly during encoding and maintenance.

Because building a mental representation of a visual scene involves processing object identity (for example colour) and location, our VSTM task required encoding both visual attributes. Given the purported role of the posterior parietal cortex in visual feature integration[23,24], it is strategically positioned to build such integrated scene representations. However, ample evidence indicates that object identity and location are preferentially processed in ventral (occipito-temporal) and dorsal (parietal) cortical visual streams, respectively[25]. It is therefore possible that at least partly distinct neural substrates underlie object and spatial VSTM capacity limits. An additional experiment investigated whether the IPS/IOS would still be involved in VSTM when only a judgement of object identity is required. This task was identical to the first experiment except that the location information was rendered task-irrelevant by always presenting the probe disc at fixation. Activation in the IPS/IOS ROI was still load-dependent ($F_{5,15} = 3.72$, $P < 0.05$, $n = 4$) and was correlated with the K function ($r = 0.70$, $t_3 = 3.67$, $P < 0.05$), indicating that the IPS/IOS might be involved in several forms of VSTM storage.

Do other brain regions besides IPS/IOS track VSTM storage capacity? To address this issue, we analysed the BOLD response in the two additional brain regions that emerged when the statistical parametric threshold was relaxed tenfold in the initial functional magnetic resonance imaging (fMRI) experiment (Fig. 3b, c): the anterior cingulate (AC) cortex and a region of ventral–occipital (VO) cortex with Talairach coordinates (Fig. 3) consistent with those of V4, an extrastriate area involved in colour processing[26]. The

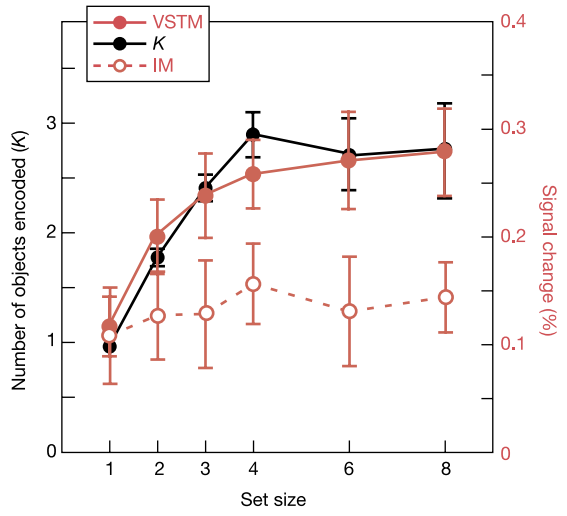

Figure 2 Behavioural performance and IPS/IOS response functions in VSTM and IM experiments. Behavioural performance corresponds to the estimated number (K) of encoded coloured discs at each set size. IPS/IOS BOLD signal response was measured at peak 5.6 s after stimulus presentation.

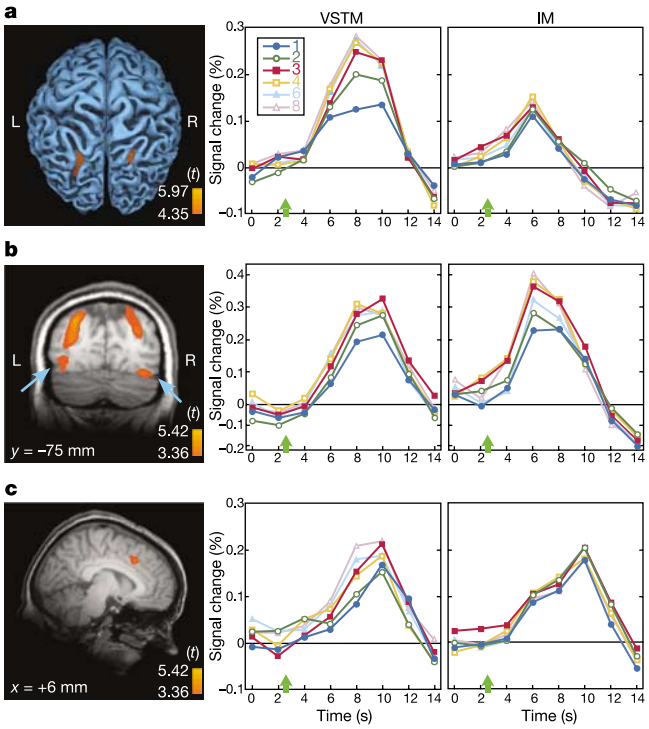

Figure 3 Brain activation time courses. Left, statistical parametric maps overlaid on structural scans of a representative subject. Middle and right, time courses for each set size in the VSTM and IM experiments, respectively. **a**, Bilateral IPS/IOS. Talairach coordinates (x, y, z): right/left, +23/−22 −59/−65 +45/+42. **b**, Bilateral VO ROI (blue arrows) with IPS/IOS activation dorsally. Right/left, +32/−34 −77/−68 −9/0. **c**, AC ROI, +8 +19 +30. The green arrow indicates the time of presentation of the visual stimulus. Although the activation baselines were variable across set sizes for VO and AC, the same statistical results are obtained when all time courses are further normalized to 0 at stimulus onset.

peak BOLD response functions of these two regions were distinct from the IPS/IOS (AC, $P < 0.001$; VO, $P < 0.05$), but not from a linear function (AC, $P = 0.40$; VO, $P = 0.13$). Additionally, neither AC nor VO showed a sustained response during maintenance in the extended VSTM retention experiment ($P > 0.05$; Fig. 4b, c), and both regions responded equally strongly under IM and VSTM conditions (P values > 0.05; Fig. 3b, c), indicating that their VSTM-related activations might be largely accounted for by perceptual and/or response components of the task. This is especially true for VO cortex, which, in stark contrast to the IPS/IOS, still showed a strong set size effect under IM conditions alone ($F_{1,5} = 4.48$, $P < 0.005$), indicating that ventral visual cortex might be driven by the perceptual load of the scene rather than by the amount of information that can be held in VSTM about the scene.

Although our results provide little evidence that the capacity limit of VSTM storage is a distributed property of the working-memory network[6,7,21], they do not exclude the possibility of additional neural contributions below the level of fMRI detection, nor are they inconsistent with the established role of the frontal/prefrontal cortex in working memory[14,20,21]. Whereas the posterior parietal cortex might act as a capacity-limited store for the representation of the visual scene, the frontal/prefrontal cortex might be necessary for the consolidation and/or maintenance of this store[18,27], especially during extended retention intervals.

Whatever the contributions of other brain regions might be, this series of experiments points to the posterior parietal cortex as a key neural locus of our impoverished mental representation of the visual world. Consistent with this notion, intraparietal cortex activity correlates with successful detection of a change between visual scenes[28], and the response of neurons in this area depends highly on the task relevance or saliency of stimuli in a multi-object display, a result that has led to the suggestion that scenes are sparsely represented in posterior parietal cortex[29]. It is tempting to speculate that, because of the severe storage capacity limit of VSTM, the posterior parietal cortex's representation of the visual world could be nothing else but sparse. □

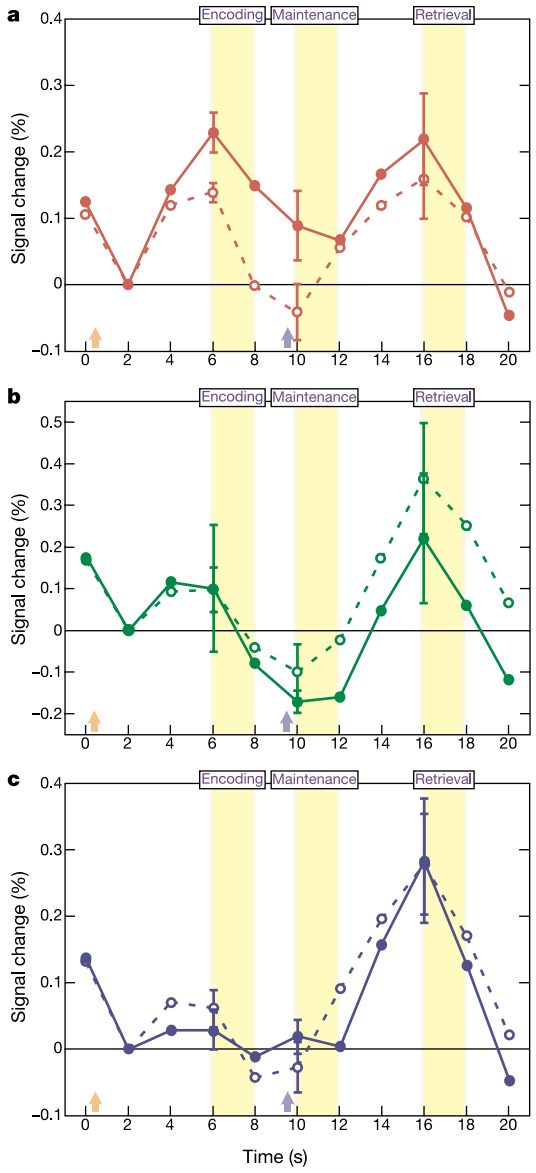

Figure 4 Response time courses during the encoding, maintenance and retrieval phases of a VSTM task with extended retention interval (9,200 ms). **a**, IPS/IOS; **b**, VO; **c**, AC. One (open circles) or three (filled circles) coloured discs were presented 1.6 s (orange arrow) before the standardized volume (time = 0 s). The purple arrow indicates the presentation of the probe display.

Methods

Subjects

Seventeen right-handed young adults (nine females) with normal or corrected-to-normal vision participated for financial compensation.

Task design

For the fast event-related fMRI experiment, each 8-s trial began with the auditory presentation, for 250 ms each, of the two digits to be rehearsed, followed by a 250-ms blank interval and a 250-ms auditory mask. At 1,500 ms after the auditory mask, the VSTM task began with presentation of the sample display for 150 ms (to preclude eye movements), with the display containing one, two, three, four, six or eight 0.38° discs, each of a different colour (either white, black, dark blue, light blue, orange, yellow, red, pink, dark green or light green), distributed among nine possible locations in a 3 × 3 matrix (1.38° × 1.38°). After a 1,200-ms retention period, a probe-coloured disc appeared for 1,750 ms at one of the occupied positions in the sample display. Subjects indicated by button press whether the probe's colour matched that of the sample. Half the trials were matched. For the other (unmatched) half, the probe colour was selected with equal probability from the other colours in the sample display or from the remaining colour set. After the visual probe response, two digits appeared for 1,500 ms and subjects indicated by button press whether the digits were identical to those rehearsed. Each fMRI run included seven iterations of each of the seven trial types (six set sizes and a non-event trial with no visual or auditory stimuli presented), with the order of trial type counterbalanced[30] within runs (seven runs per session).

For the slow event-related fMRI experiment. Six right-handed subjects (three females) from the pool of 17 subjects performed an additional experiment that was identical to the first except that the retention interval was extended from 1,200 to 9,200 ms (trial duration 18 s; seven trials per fMRI run) and trial types were randomly intermixed.

fMRI methods

Anatomical low-resolution and three-dimensional high-resolution T1-weighted images were acquired with conventional parameters on a 3-T GE MRI system (Milwaukee, Wisconsin, USA). Nineteen 7-mm-thick (3.75 mm × 3.75 mm in-plane, 0 mm skip) axial slices were taken parallel to the AC–PC line. T2*-weighted image parameters: echo time 25 ms; flip angle 70°; field of view 24 cm; 64 × 64 matrix; repetition time 2,000 ms. Trials were triggered by scanner pulses and presented with PsychToolBox for Matlab on an Apple G4 Macintosh. Stimuli were back-projected from an LCD projector on to a screen viewed through a prism mirror by the supine subject in the MR scanner.

Data analysis

For behavioural data, the number of objects encoded was estimated by using Cowan's K formula[11]: for each set size, K = (hit rate + correct rejection rate − 1)N, where K is the number of objects encoded and N is the number of objects presented. This formula yields similar estimates to those obtained by related formulae[12,13] and by full report (R.M., J.J.T. and C. M. Gilbert, unpublished observations).

For fMRI data, image analysis was performed with BrainVoyager 4.9.1 (Brain Innovation, Maastricht, The Netherlands). Data preprocessing included image realignment, three-dimensional motion correction, linear detrending, correction for slice scan acquisition order, and spatial smoothing with an 8-mm gaussian kernel (full width at half-maximum). Statistical parametric maps of BOLD activation for the fast event-related experiment were created by using a multiple regression analysis, with regressors defined for each trial type and convolved with a canonical haemodynamic function. The regression coefficients for each set size were weighted by their respective K estimates (balanced contrast design). The resulting maps from all subjects were standardized into Talairach space and superimposed to create cluster-filtered (equivalent of six contiguous 100-mm^3 voxels in original space) composite maps. The overall model fit was assessed with an F value, and the obtained P values were corrected for the number of comparisons

(http://afni.nimh.nih.gov/afni/) with a random-effects model. Time courses of each of the six set size conditions were extracted from each ROI to compute their respective percentage signal changes, with the no-event time series as baseline[30], first within each subject and subsequently averaged across subjects. The peak percentage signal change for each ROI was derived by collapsing the time courses of all set sizes and subjects and determining the time point of greatest signal amplitude in the grand average. One subject with unsteady raw signal who failed to show any time-locked response was removed from further analysis. The slow event-related experiment was analysed as above, except that the percentage signal change of each time course was normalized to the first image acquired after stimulus presentation (baseline), because the signal from the previous image still included the falling phase of the response to the previous trial (Fig. 4). The peaks of the encoding, maintenance and retrieval phases corresponded to the volumes acquired 5.5–7.5, 9.5–11.5 and 15.5–17.5 s after stimulus presentation[21], respectively.

Received 11 January; accepted 9 March 2004; doi:10.1038/nature02466.

1. Rensink, R. A. Change detection. *Annu. Rev. Psychol.* **53,** 245–277 (2002).
2. Simons, D. & Levin, D. Change blindness. *Trends Cogn. Sci.* **1,** 261–267 (1997).
3. Chun, M. M. & Potter, M. C. A two-stage model for multiple target detection in rapid serial visual presentation. *J. Exp. Psychol. Hum. Percept. Perform.* **21,** 109–127 (1995).
4. Jolicoeur, P., Dell' Acqua, R. & Crebolder, J. M. in *The Limits of Attention: Temporal Constraints in Human Information Processing* (ed. Shapiro, K.) 82–99 (Oxford Univ. Press, 2001).
5. Wheeler, M. E. & Treisman, A. M. Binding in short-term visual memory. *J. Exp. Psychol. Gen.* **131,** 48–64 (2002).
6. Goldman-Rakic, P. S. in *Handbook of Physiology: The Nervous System, Higher Functions of the Brain* (eds Mountcastle, V. B. & Plum, F.) 373–417 (American Physiological Society, Bethesda, Maryland, 1987).
7. Ungerleider, L. G., Courtney, S. M. & Haxby, J. V. A neural system for human visual working memory. *Proc. Natl Acad. Sci. USA* **95,** 883–890 (1998).
8. Callicott, J. H. *et al.* Physiological characteristics of capacity constraints in working memory as revealed by functional MRI. *Cereb. Cortex* **9,** 20–26 (1999).
9. Linden, D. E. *et al.* Cortical capacity constraints for visual working memory: Dissociation of fMRI load effects in a fronto-parietal network. *Neuroimage* **20,** 1518–1530 (2003).
10. Duncan, J. *et al.* Systematic analysis of deficits in visual attention. *J. Exp. Psychol. Gen.* **128,** 450–478 (1999).
11. Cowan, N. The magical number 4 in short-term memory: A reconsideration of mental storage capacity. *Behav. Brain Sci.* **24,** 87–114 (2001).
12. Pashler, H. Familiarity and visual change detection. *Percept. Psychophys.* **44,** 369–378 (1988).
13. Vogel, E. K., Woodman, G. F. & Luck, S. J. Storage of features, conjunctions and objects in visual working memory. *J. Exp. Psychol. Hum. Percept. Perform.* **27,** 92–114 (2001).
14. Cohen, J. D. *et al.* Temporal dynamics of brain activation during a working memory task. *Nature* **386,** 604–608 (1997).
15. Phillips, W. A. On the distinction between sensory storage and short-term visual memory. *Percept. Psychophys.* **16,** 283–290 (1974).
16. Coltheart, M. in *New Horizons in Psychology* (ed. Dodwell, P. C.) 62–85 (Harmondsworth, Penguin, 1972).
17. Baddeley, A. Working memory. *Science* **255,** 556–559 (1992).
18. Smith, E. E. & Jonides, J. Neuroimaging analyses of human working memory. *Proc. Natl Acad. Sci. USA* **95,** 12061–12068 (1998).
19. Rosnow, R. L. & Rosenthal, R. Contrasts and interactions redux: Five easy pieces. *Psychol. Sci.* **7,** 253–257 (1996).
20. Courtney, S. M., Ungerleider, L. G., Keil, K. & Haxby, J. V. Transient and sustained activity in a distributed neural system for human working memory. *Nature* **386,** 608–611 (1997).
21. Pessoa, K., Gutierrez, E., Bandettini, P. A. & Ungerleider, L. G. Neural correlates of visual working memory: fMRI amplitude predicts task performance. *Neuron* **35,** 975–987 (2002).
22. Zarahn, E., Aguirre, G. & D'Esposito, M. A trial-based experimental design for fMRI. *Neuroimage* **6,** 122–138 (1997).
23. Friedman-Hill, S. R., Robertson, L. C. & Treisman, A. Parietal contributions to visual feature binding: Evidence from a patient with bilateral lesions. *Science* **269,** 853–855 (1995).
24. Shafritz, K. M., Gore, J. C. & Marois, R. The role of the parietal cortex in visual feature binding. *Proc. Natl Acad. Sci. USA* **99,** 10917–10922 (2002).
25. Haxby, J. V. *et al.* Dissociation of object and spatial visual processing pathways in human extrastriate cortex. *Proc. Natl Acad. Sci. USA* **88,** 1621–1625 (1991).
26. McKeefry, D. J. & Zeki, S. The position and topography of the human colour centre as revealed by functional magnetic resonance imaging. *Brain* **120,** 2229–2242 (1997).
27. Curtis, C. E. & D'Esposito, M. Persistent activity in the prefrontal cortex during working memory. *Trends Cogn. Sci.* **7,** 415–423 (2003).
28. Beck, D. M., Rees, G., Frith, C. D. & Lavie, N. Neural correlates of change detection and change blindness. *Nature Neurosci.* **4,** 645–650 (2001).
29. Gottlieb, J. P., Kusunoki, M. & Goldberg, M. E. The representation of visual salience in monkey parietal cortex. *Nature* **391,** 481–484 (1998).
30. Kourtzi, Z. & Kanwisher, N. Representation of perceived object shape by the human lateral occipital complex. *Science* **293,** 1506–1509 (2001).

Acknowledgements We thank I. Gauthier, M. Chun, G. Logan and J. Schall for comments on earlier versions of this manuscript, and D. Nikolaiczyk-Stocks and A. Snyder for expert technical assistance. This work was supported by a grant from the NSF to R.M.

Competing interests statement The authors declare that they have no competing financial interests.

Correspondence and requests for materials should be addressed to R.M. (rene.marois@vanderbilt.edu).

The endothelial-cell-derived secreted factor *Egfl7* regulates vascular tube formation

Leon H. Parker[1], Maike Schmidt[1], Suk-Won Jin[3], Alane M. Gray[1], Dimitris Beis[3], Thinh Pham[2], Gretchen Frantz[2], Susan Palmieri[2], Kenneth Hillan[2], Didier Y. R. Stainier[3], Frederic J. de Sauvage[1] & Weilan Ye[1]

[1]*Molecular Biology Department and* [2]*Pathology Department, Genentech Inc., South San Francisco, California 94080, USA*
[3]*Department of Biochemistry and Biophysics, Programs in Developmental Biology, Genetics and Human Genetics, University of California San Francisco, San Francisco, California 94143-0448, USA*

Vascular development is a complex but orderly process that is tightly regulated. A number of secreted factors produced by surrounding cells regulate endothelial cell (EC) differentiation, proliferation, migration and coalescence into cord-like structures[1,2]. Vascular cords then undergo tubulogenesis to form vessels with a central lumen[3,4]. But little is known about how tubulogenesis is regulated *in vivo*. Here we report the identification and characterization of a new EC-derived secreted factor, *EGF-like domain 7* (*Egfl7*). *Egfl7* is expressed at high levels in the vasculature associated with tissue proliferation, and is downregulated in most of the mature vessels in normal adult tissues. Loss of *Egfl7* function in zebrafish embryos specifically blocks vascular tubulogenesis. We uncover a dynamic process during which gradual separation and proper spatial arrangement of the angioblasts allow subsequent assembly of vascular tubes. This process fails to take place in *Egfl7* knockdown embryos, leading to the failure of vascular tube formation. Our study defines a regulator that controls a specific and important step in vasculogenesis.

Tubulogenesis is an essential step in vascular development. Vascular tube formation proceeds through two phases: first, ECs coalesce to form cords after they reach their destination; cords are then reshaped into tubes[3,4]. But we have little understanding of how vascular cords progress to become tubes and what factors regulate this transition *in vivo*. In an effort to identify molecules involved in the regulation of vascular development, we examined the expression pattern of more than 600 new secreted and transmembrane factors by *in situ* hybridization in whole mouse embryos ranging from embryonic day 7.5 (E7.5) to E14.5, a time window encompassing many key steps in vasculogenesis (vessel formation from EC progenitors) and angiogenesis (sprouting from existing vessels)[1,2,5]. One of the factors we identified in this screen is a secreted factor known as *EGF-like domain 7* (*Egfl7*, also called *zneu1*, *neu1*, *notch4-like*, *tango125*, *VE-statin*).

Egfl7 encodes a putative secreted protein with a relative molecular mass of ~30 K that is evolutionarily conserved. The EGFL7 protein contains a signal sequence, an EMI domain at the amino terminus (the EMI domain is present in a number of extracellular-matrix-associated proteins involved in regulating cell adhesion[6,7]), followed by two EGF-like domains and a leucine- and valine-rich carboxy-terminal region (Supplementary Fig. 1a). The mammalian *Egfl7* belongs to a small gene family. Through BLAST searches, we identified one closely related gene, *Egfl8*, which has a domain organization identical to that of *Egfl7*. Interestingly, this gene family seems to be more complex in mammals, as we have not been able to identify an *Egfl8* orthologue in several fish genomes (*Danio rerio*, *Medaka* and *Fugu*) (Supplementary Fig. 1c).

The expression pattern of *Egfl7* is conserved across species. In mouse, human and zebrafish embryos, high levels of *Egfl7* transcripts are detected in endothelial progenitors and ECs in all vessels